Energy Storage Materials 53 (2022) 638–645

Contents lists available at ScienceDirect

Energy Storage Materials

journal homepage: www.elsevier.com/locate/ensm

Trace amounts of fluorinated surfactant additives enable high performance zinc-ion batteries

Fangjia Zhao [a], Zhuanfang Jing [b], Xiaoxia Guo [a], Jianwei Li [a], Haobo Dong [a], Yeshu Tan [a], Longxiang Liu [a], Yongquan Zhou [b], Rhodri Owen [c], Paul R. Shearing [c], Dan J.L. Brett [c], Guanjie He [a,c,*], Ivan P. Parkin [a,*]

[a] Christopher Ingold Laboratory, Department of Chemistry, University College London, 20 Gordon Street, London WC1H 0AJ, UK
[b] Key Laboratory of Comprehensive and Highly Efficient Utilization of Salt Lake Resources, Qinghai Institute of Salt Lakes, Chinese Academy of Sciences, Qinghai 810008, China
[c] Electrochemical Innovation Lab, Department of Chemical Engineering, University College London, London WC1E 7JE, UK

ARTICLE INFO

Keywords:
Zinc ion battery
Electrolyte additive
Perfluorooctanoic acid
Zinc dendrites
Electrolyte

ABSTRACT

Aqueous zinc-ion batteries are promising alternatives to lithium-ion batteries for grid-scale energy storage. However, the practical application of AZIBs is challenged by side reactions and unsatisfactory performance. Electrolyte additives are reported that can inhibit side reactions on the Zn anode and enlarge the working potential window of aqueous electrolytes. Here we propose that trace amounts of perfluorooctanoic acid (PFOA) can facilitate long-term reversible Zn deposition in AZIBs due to perfluorinated n-octyl chains ordered orientation adsorbing on the electrode surface. Benefitting from its intrinsic surfactant properties, PFOA additives can reduce the surface tension of electrolytes and improve the wettability of electrolytes on the electrode. Symmetric Zn cells survived up to 2200 hours owing to the self-adjusting absorption layer. The molecular dynamics results show that the as-formed electronegative adsorption layer acts as a zincophilic layer to regulate the ions in the electrolyte. With adding PFOA, the electrochemical stability window of aqueous electrolyte enlarged to 2.1 V. Owing to the ultra-low additive usage amount, this strategy provides a facile and low-cost method to tackle common issues in AZIBs.

1. Introduction

Driven by low carbon emission targets, research into sustainable energy harvesting devices are attracting increasing interest. The market size reached $ 0.613 billion in 2020 and is projected to reach $ 1129 billion by 2027. Low-cost and efficient energy storage technologies play essential roles in balancing the gap between electricity peak and off-peak demands. Benefiting from its intrinsic high energy density and long lifespan, rechargeable lithium-ion batteries are leading the secondary battery market. However, the safety concern of organic electrolytes in lithium-ion batteries and the growing price of lithium battery component sources drive research into alternative technologies such as aqueous batteries for next-generation grid-scale energy storage devices [1–3]. Among them, aqueous zinc-ion batteries (AZIBs) benefit from the intrinsic properties of zinc, including high theoretical volumetric and gravimetric capacities of 5855 mAh cm^{-3} and 820 mAh g^{-1}, respectively, suitable redox potential (-0.76 V *vs.* standard hydrogen electrode), low cost, and high abundance. These properties make AZIBs safe, low-cost, and efficient candidates for practical applications.

Although AZIBs have achieved a significant progress in energy storage fields, there are two remaining issues that AZIBs face; one is the relatively low working potential window. Enlarging the working window can enable more redox reactions and thus achieve higher energy density. The other is rich solution-related side reactions. Since the reduction potential of Zn^{2+}/Zn is more negative than that of the hydrogen evolution reaction (HER), the water can be reduced to H_2 during the zinc deposition, which creates an alkaline corrosive environment at the interface between zinc and electrolyte. The inhomogeneous corrosion byproducts will reduce the Coulombic efficiency of zinc plating and stripping and further induced zinc dendrite growth that may lead to separator penetration and battery short-circuiting.

Great efforts have been devoted to suppress side reactions and

* Corresponding authors at: Christopher Ingold Laboratory, Department of Chemistry, University College London, 20 Gordon Street, London WC1H 0AJ, UK.
E-mail addresses: g.he@ucl.ac.uk (G. He), i.p.parkin@ucl.ac.uk (I.P. Parkin).

https://doi.org/10.1016/j.ensm.2022.10.001
Received 7 May 2022; Received in revised form 8 August 2022; Accepted 1 October 2022
Available online 2 October 2022

regulate the dendrite growth on the zinc anode to achieve reversible zinc stripping and plating [4–8]. Previous strategies include (i) electrolyte additives, such as sodium dodecyl sulfate [9], tetrabutylammonium sulfate [10], arginine [11] and lithium chloride [12]; (ii) surface/interface nanoscale modification [13,14], such as building 3D interconnected ZnF_2 matrix [15], controlling preferential zinc lattice planes [16] and coating polymer glue protective layers on the zinc anode [17], and (iii) highly concentrated electrolytes including Zn molten hydrates [18], and trifluoromethanesulfonate [19,20]. These strategies have been proven to expand the lifespan of zinc anodes and increase battery stability by forming solid electrolyte interphases (SEI). However, the volume change during zinc plating and stripping could lead to the failure of the anode due to cracking or inhomogeneous distribution of the SEI [21]. More importantly, expensive salts and complicated modification methods will undermine the advantages of the low-cost nature of AZIBs. Therefore, cost-effective electrolyte additives are desirable to solve these problems [22,23]. Additionally, interfacial absorption and electrostatic shielding enable the regulating of Zn^{2+} flux and achieve reversible zinc plating. Although numerous additives have been studied for AZIBs, considering the gravimetric energy density of battery system, the amount of electrolyte additive needs to be considered for grid storage devices design.

In this work, a non-sacrificial fluorinated additive with ultra-low amount was investigated by combining experimental measurements with theoretical simulations. The results show that PFOA additives can enable a stable zinc plating/stripping process and enlarge the working window of electrolyte for AZIBs. Owing to the PFOA additives adsorption layer with strong electronegative perfluoroalkyl chains, the Zn^{2+} flux near electrode/electrolyte interface can be redistributed and the sulfate anion migration to the zinc anode is inhibited. Benefiting from the hydrophobic nature of long perfluorinated carbon chains in PFOA additives, the working window of the electrolyte can be enlarged to 2.1 V due to the limited free water molecular near PFOA adsorption layer, and thus water related side reactions were suppressed. In addition, owing to the intrinsic trend of the absorbed surfactant on the electrode surface, the consequently self-adjusting PFOA chain could tolerate the volume change of the anode during Zn plating/stripping even at a high current density of 10 A g^{-1}. The enhanced anti-corrosion and uniform deposition process of the electrolyte with PFOA additives were directly illustrated using *in situ* optical microscopy and confirmed by soaking experiment. Besides, due to suppressed side reactions, higher Coulombic efficiency is achieved using Zn||Cu cells. Consequently, the electrolyte with PFOA additives delivers long-term (2200 h) reversible deposition in zinc symmetric cells and a high rate performance of 153 mAh g^{-1} in Zn||$Na_{0.65}Mn_2O_4$ cells under a high current density of 5 A g^{-1}.

2. Results and discussion

The schematic illustration of PFOA molecules absorption process on the zinc anode was provided in Fig. 1. As amphiphilic molecules, PFOA surfactant consists of a hydrophilic carboxylate head group and a hydrophobic perfluorinated n-octyl tail group. Compared with water moleculars, surfactants proceed through a low energy barrier method to reach the interface and adsorb on the interface via intermolecular interaction. The polyfluoroalkyl acetate (Figs. S2 and S3) could bind to Zn^{2+} through the acetate group and help fill the coordination sphere displacing SO_4^{2-}. The polyfluoroalkyl chains in PFOA additives are hydrophobic and can limit the water-involved side reactions on the zinc anode. Water molecules and SO_4^{2-} need to overcome extra energy barriers to pass through the adsorption layer on the Zn anode surface, and thus water-related side reactions including HER and oxygen evolution reaction (OER) can be inhibited. As a consequence, zinc plating starts with smaller nuclei and smooth plating is achieved.

The mechanism of PFOA additives on zinc anodes was evaluated by various spectroscopic techniques. X-ray photoelectron spectroscopy (XPS), Fourier-transform infrared spectroscopy (FTIR), and Energy dispersive spectrometry (EDS) were applied to verify the adsorption behavior of PFO- on the zinc surface. F 1s XPS spectrum is presented in Fig. 2a. The presence of -CF_2 (688.9 eV) could support molecular adsorption of PFOA on the zinc surface. As shown in Fig. S4, after soaking in PFOA solution, zinc foil displays C-F stretching in the range 1000–1400 cm^{-1}, which is original from the adsorption of PFOA perfluorinated n-octyl tail. Besides, the EDS mapping results (Fig. S5) show an even distribution of C and F signal, confirming the even adsorption of PFOA molecular on zinc anode surface. To clarify the environmental change in electrolyte after the addition of PFOA, FTIR spectral characterization were performed(Fig. S6). The intensity of SO_4^{2-} broad band peak located at 1085 cm^{-1} reduced after the addition of PFOA in electrolyte, illustrating that PFOA could interact with sulfate anion and limit the migration of sulfate anion in the electrolyte, which also paves the

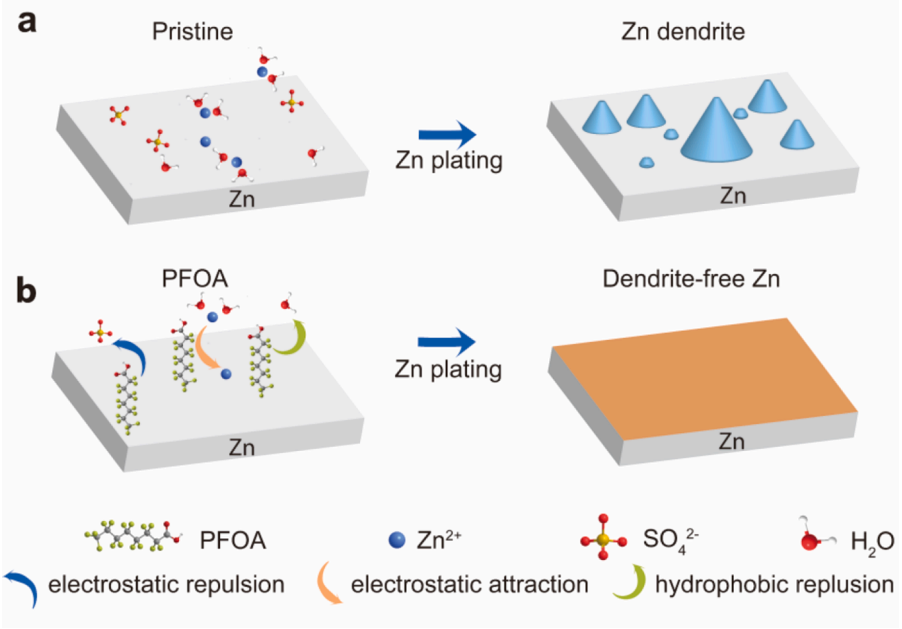

Fig. 1. Schematic diagram of ions in (a) pristine electrolyte and (b) electrolyte with PFOA additives.

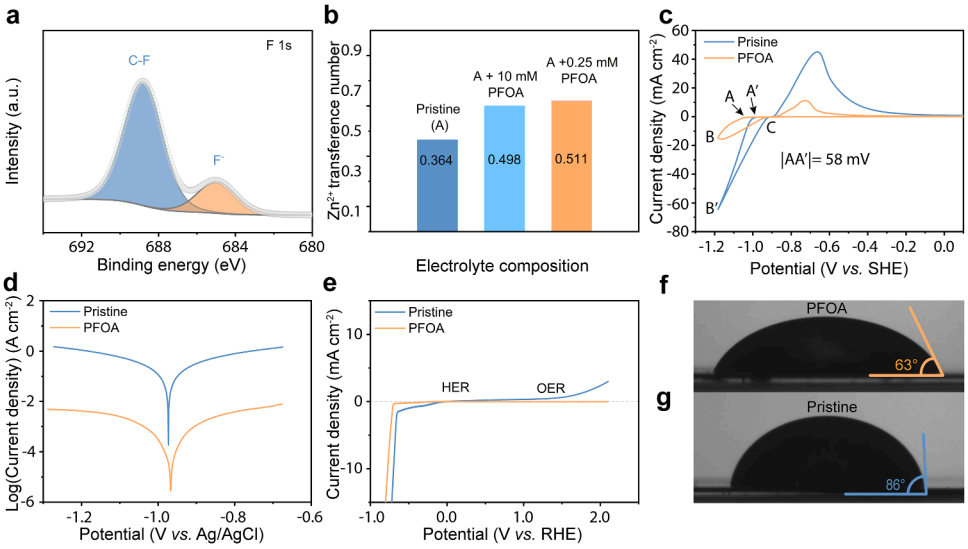

Fig. 2. Properties of electrolyte with PFOA additives. (a) F 1s XPS spectrum of a zinc anode after cycling in the electrolyte with PFOA additives. (b) Zn transference number at various electrolyte compositions. (c) Zn symmetric plating and stripping cyclic voltammetry (CV) curves in electrolyte with PFOA additives at a scan rate of 1 mV s^{-1}. (d) Linear polarization curves of Zn foil in the pristine electrolyte (3 M $ZnSO_4$) and PFOA (3 M $ZnSO_4$ and 0.25 mM PFOA) electrolyte. (e) The working window of different electrolytes. (f, g) The contact angle on zinc substrates using different electrolytes.

way for Zn^{2+} fast migration in the electrolyte. The enhanced zinc ion migration was further confirmed by comparing Zn^{2+} transference number in different electrolytes (Fig. 2b). PFOA additives exhibits a higher zinc transference number of 0.511 (Fig. S7) compared with 0.364 of the pristine electrolyte (Fig. S9), illustrating that PFOA additives could facilitate sufficient ion transport in electrolytes. Considering the balancing of usage amount, electrolyte pH value (Fig. S10) and electrolyte surface tension (Fig. S11), 0.25 mM of PFOA was added into the pristine electrolyte in experiments (noted as PFOA in figures). The low addition amount of electrolyte additive also contributes to the mass weight of the whole battery and meets the practical demand. It is well-known that the initial nucleation size has significant effects on the zinc plating and stripping process. To further investigate the initial nucleation behavior in electrolyte with PFOA additives on the electrode/electrolyte interface. Cyclic voltammetry (CV) test was performed in a two-electrode configuration, Ti foil was employed as working electrode while Zn foil acted as counter electrode and reference electrode. When the potential sweep towards the positive side, a crossover characteristic of nucleation processes was shown in Fig. 2c. Point A stand for the potential that Zn^{2+} ions plating begins and crossover point B stand for the crossover potential. The gap between the plating point (A) and crossover point (B) shows the nucleation overpotential (NOP). By comparing the NOP difference, the extent of zinc plating polarization and the effect of additives in electrolytes could be illustrated [24]. According to the previous research, the relationship between critical Zn nucleus radius (r_{crit}) and NOP obeys the following equation [25–27]:

$$r_{crit} = 2\frac{\gamma V_m}{F|\eta|}$$

Where γ is the surface energy of the Zn-electrolyte interface, V_m is the molar volume of Zn, F is Faraday's constant, and η is the NOP. It is known that the Zn deposition would be processed more orderly with a higher NOP value [28]. In comparison with the pristine electrolyte, electrolyte with PFOA additives increases the NOP value by 58 mV, which has been mainly contributed by the coordination between hydrated Zn^{2+} ions and PFOA additives. The increased overpotential is due to optimized zinc nucleation and growth scales with finer nuclei. Furthermore, the absorption of PFOA additives with perfluorinated n-octyl tails on the electrode/electrolyte interface could boost the zinc anode zincophilicity and redistribute the Zn^{2+} ion flux, thus avoiding the uneven distribution of charges caused by "tip effect". The corrosion resistance ability is essential to evaluate the interface stability between electrode and electrolyte. As shown in Fig. 2d, the corrosion current is lower in the electrolyte with PFOA additives, thereby enhancing the corrosion resistance. Also, the corrosion happens at a more positive potential with PFOA additives, illustrating enhanced corrosion resistance. Meanwhile, as the electron withdrawing group could reduce electron density in molecules through the carbon atom bonds to electronegative atoms like fluorine, PFOA molecular have polyfluoroalkyl chains with C-F bond, it has been demonstrated that adding surfactants to the electrolyte could affect the working window of electrolyte. The electrochemical stability window of the aqueous electrolytes was investigated by linear sweep voltammetry, as shown in Fig. 2e. The anodic scans and cathodic scans were carried out using Ti electrodes. As observed in the polarization curves of the cathodic scans at a scan rate of 10 mV s^{-1}, the onset potential of HER was suppressed in the electrolyte with PFOA additives (-0.69 V *vs.* RHE), higher than that in the pristine electrolyte (-0.64 *vs.* RHE). As for the OER, the onset potential shifted from 1.7 V to 2.1 V, illustrating that the working window of the aqueous electrolyte is expanded, and less gas was generated on the interface, which is beneficial for long-term stability. Furthermore, due to a lack of electrostatic/hydrogen bonding, the intermolecular force between PFOA molecules and water molecules is much lower than that within water molecules [29], and thus trace amount of PFOA additives can change the surface tension of electrolyte from 72 mN m^{-1} to below 35 mN m^{-1}(Fig. S11). As a result, the wettability of electrolytes on both zinc anodes and cathodes were improved. The surface wettability of different electrolytes on Zn anodes were characterized using contact angle measurement. Different from the relatively hydrophobic results of the pristine electrolytes on Zn anodes, the lower contact angle value of electrolytes with PFOA additives (61°) shows that PFOA additives increased the wettability of electrolyte on the Zn anode (Fig. 2f) and thus Zn^{2+} is more feasible to reach the Zn anode surface[30]. The enhanced wettability of electrolyte with PFOA additives on the cathode part was shown in Fig. S12.

To directly probe the anti-corrosion effect of PFOA additives, zinc anode soaking experiments (Figs. S13–S15) were conducted. Obvious hydrogen bubble could be observed after immersing zinc anode in pristine electrolyte for 12 hours, showing that the mild acid environment of 3 M $ZnSO_4$ could irrosion the zinc anode. In contrast, no hydrogen bubbles were spotted on zinc foil in electrolyte with PFOA additives, indicating that H_2O penetration were suppressed and less corrosion happened at the interface. Besides, to directly monitor the zinc plating process on zinc anode in different electrolytes, *in situ* optical microscopy observation (Fig. S16) was conducted under a current density of 5 ma cm^{-2}. Zinc dendrites begin to generate on zinc after 2 min. With increasing the deposition time, the deposited zinc shows a highly

dendritic and mossy morphology. In contrast, homogeneous zinc deposition is achieved in electrolyte with PFOA additives, confirming the effective regulation of PFOA additives to zinc deposition process.

To further evaluate the electrochemical performance of batteries in the electrolyte with PFOA additives [31,32], the Coulombic efficiency (CE) of Zn plating and stripping processes was explored on the Cu substrate under 0.4 mA cm^{-2}. Fig. 3a shows that after the initial nucleation process, the CE of the zinc plating and stripping process in the electrolyte with PFOA additives is highly stable (98%), which agrees with the previous observation that PFOA additives could contribute to the Zn plating process. In comparison, CE in the pristine electrolyte shows a fluctuation (Figs. S18 and S19) after 50 cycles and the CE is relatively low (96%) due to severe side reactions. Furthermore, the voltage-time curves of electrolytes with PFOA additives (Figs. S20 and S21) is more stable, indicating that the adsorption layer of PFOA additives is self-adaptable and could tolerate the morphology change during Zn plating and stripping processes. To further verify the tolerance and polarization of the electrolyte with PFOA additives under various current densities, Zn-Zn symmetric cells were assembled and tested at stepwise current densities from 0.2 to 10 mA cm^{-2} and back to 0.2 mA cm^{-2} (Fig. 3b). Remarkably, the Zn plating and stripping overpotentials in the electrolyte with PFOA additives are lower than in the pristine electrolyte especially under the high current density of 10 mA cm^{-2}. Besides, the electrolyte with PFOA additives operates at a steady overpotential while the pristine electrolyte exhibited micro short-circuits in the rate performance test, indicating enhanced Zn transfer kinetics in the electrolyte with PFOA additives [27]. The highly reversible Zn plating and stripping voltage plateau in electrolyte with PFOA additives are due to the reduced water-involved side reactions on the Zn anode. To verify this hypothesis, *ex-situ* XRD of Zn anodes was evaluated by disassembling from symmetric cells after cycling 50 cycles under 1 mA cm^{-2}. XRD results in Fig. 3c show characteristic byproduct diffraction peaks located at 14.9°, 17.1°, and 25.8° correspond to $Zn_4SO_4(OH)_6{\cdot}4H_2O$ (PDF #44-0673), which is induced by the water-involved side reactions in the pristine electrolyte. In contrast, the Zn anode in the electrolyte with PFOA additive shows a clear XRD pattern of Zn without obvious byproducts peaks, indicating that PFOA additives suppress the side reactions on the Zn anode during plating and stripping. Impressively, ultralong lifespan symmetric cells can be achieved in the electrolyte with PFOA additives. As shown in Fig. 3d, Zn symmetric cells could operate steadily for 2200 h under 1 mA cm^{-2}, in contrast to the collapse of symmetric cells after 180 h in the pristine electrolyte. The electrolyte with PFOA additives maintain a low voltage hysteresis during long-term cycling, confirming the stabilizing effect of PFOA additives on the Zn plating and stripping processes. Dendrite growth is one of the major concerns for AZIBs. To further evaluate the experimental effects of PFOA additives on Zn dendrite growth, Scanning electron microscope (SEM) was used to compare the morphological evolution of Zn anodes after cycling in different electrolytes. Fig. S22 shows that dendrite growth and proliferation led to the obvious 'flower-like' Zn aggregation on the anode in the pristine electrolyte, which is in line with *ex-situ* XRD results. In contrast, Zn anodes maintained a smooth surface with dendrite-less morphology after cycling in the electrolyte with PFOA additives (Fig. 3e,f), which confirmed that PFOA additives can contribute to the uniform Zn plating and stripping.

To elucidate the effect of PFOA additives on the cycling performance of the cathode material, $Na_{0.65}Mn_2O_4$ nanorods (Fig. S23) were synthesized and utilized to fabricate the asymmetric cell [33]. The full cells were tested in the electrolyte with added 0.2 M $MnSO_4$ to avoid the dissolution of the cathode material [34,35]. Fig. 4a shows typical redox peaks of $Na_{0.65}Mn_2O_4$ cathode material in AZIBs, indicating that the PFOA molecule has no side effects on the cathode materials. Furthermore, the polarization of the full cells in the electrolyte with PFOA additives is slightly lower than the pristine electrolyte, which shows an enhanced charge transport induced by PFOA additives. Electrochemical impedance spectroscopy (EIS) was applied to further investigate the effect of the PFOA additives on inherent resistance (Fig. 4b). From the enlarged Nyquist plot, the decreased semi-circle in the electrolyte with PFOA additives tested before cycling implies that PFOA additives can improve the charge transfer ability. While R_{ct} decreased from 45.87 to 25.15 Ω with the addition of PFOA, which is in line with the reduced polarization from the CV curves. To further illustrate the charge storage mechanism, the capacitive contribution in the electrolyte with PFOA additives was studied in Fig. S24a and compared with the pristine electrolyte (Fig. S24b), which illustrated the electrolyte with PFOA additives has a higher proportion of capacitive contribution under

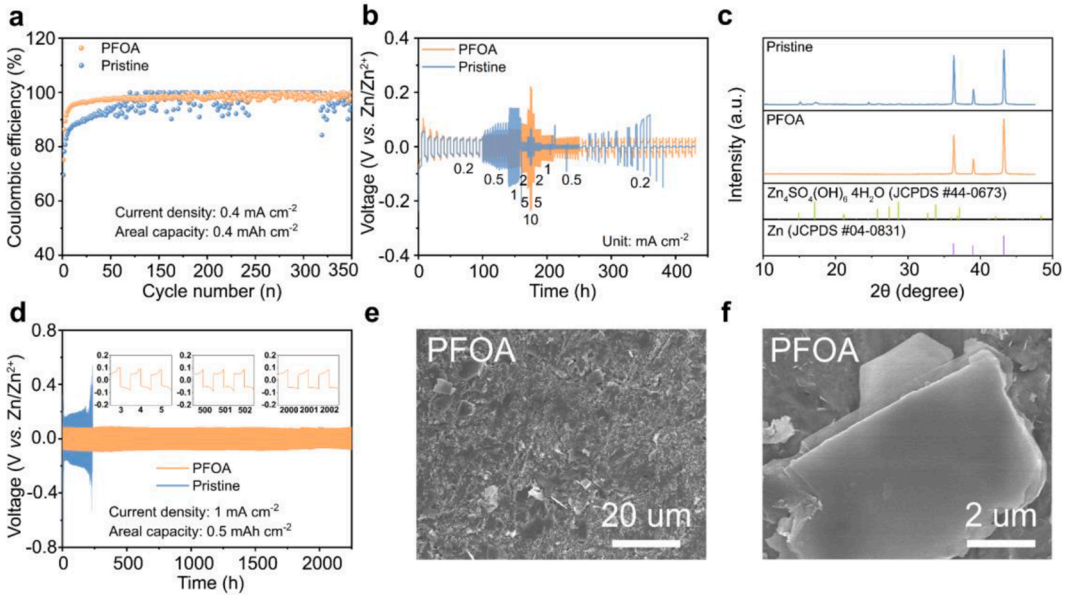

Fig. 3. (a) Coulombic efficiency using Cu||Zn cells in different electrolytes. (b) Rate performance of Zn symmetric cells measured at step up/down current densities of 0.2, 0.5, 1, 2, 5, 10, 5, 2, 1, 0.5, 0.2 mA cm^{-2}. (c) *Ex-situ* X-ray diffraction (XRD) profile of the Zn anode after cycling. (d) Long-term cycling using the Zn symmetric cell in different electrolytes under 1 mA cm^{-2}. (e, f) SEM of the Zn anode surface using Zn symmetric cells in electrolytes with PFOA additives after Zn plating and stripping for 100 cycles at a current density of 10 mA cm^{-2} and a cycling capacity of 5 mA cm^{-2}.

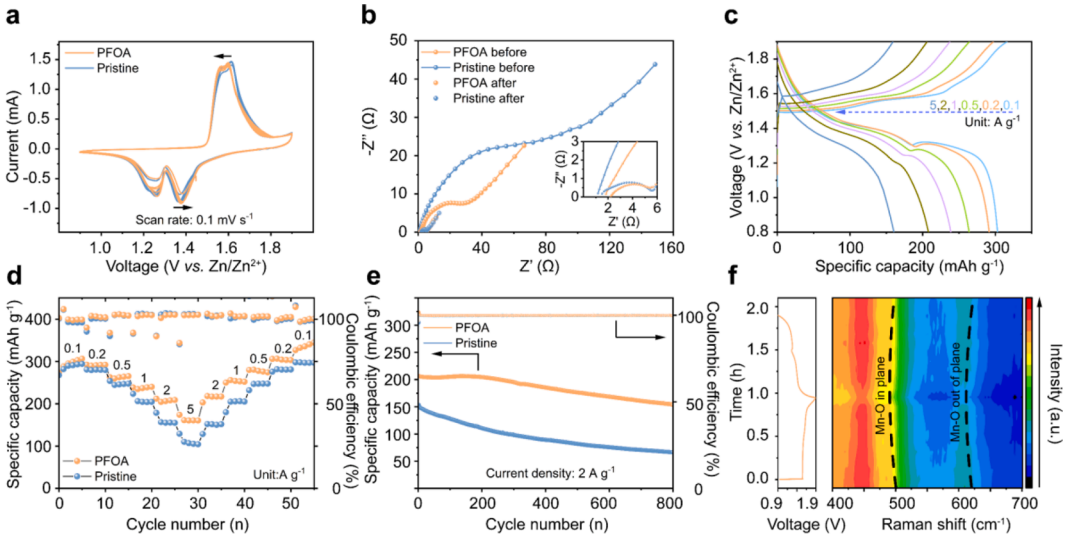

Fig. 4. Electrochemical performance of $Na_{0.65}Mn_2O_4$||Zn full cells: (a) CV curves in different electrolytes under the scan rate of 0.1 mV s^{-1}. (b) electrochemical impedance spectroscopy comparison in different electrolytes. (c) Galvanostatic charge-discharge profile under different rates. (d) rate performance in different electrolytes. (e) $Na_{0.65}Mn_2O_4$||Zn long-term cycling performance and CE in the electrolyte with and without PFOA additives under the current density of 2 A g^{-1}. (f) *In-situ* Raman spectra of the $Na_{0.65}Mn_2O_4$ cathode material during cycling in the electrolyte with PFOA additives.

different scan rates. Figs. 4c and S25 show the galvanostatic charge-discharge profile in PFOA and pristine electrolytes. The cycling and rate performance of AZIBs using different electrolytes were further illustrated in Fig. 4d, where the current density was raised stepwise from 0.1 to 5 A g^{-1} and returned to 0.1 A g^{-1} with five cycles at each current density. Impressively, $Na_{0.65}Mn_2O_4$ cathode materials using electrolyte with PFOA additives show higher specific capacity under different current densities, *i.e.,* 295, 290, 262, 236, 206, 153 mAh g^{-1} at 0.1, 0.2, 0.5, 1, 2, 5 A g^{-1}, respectively, and the recovery of capacity was achieved at different current densities with a corresponding CE of > 99%. In comparison, the specific capacity of the battery is relatively low in pristine electrolyte, that is 290, 279, 245, 204, 155, 110 mAh g^{-1} at 0.1, 0.2, 0.5, 1, 2, 5 A g^{-1}, respectively. The rate performance of the battery in the electrolyte with PFOA additives is increased especially under a high current density, i.e. 39% increase from 110 to 153 mAh g^{-1} (Fig. 4d). The long-term durability of batteries using different electrolytes was studied. As shown in Fig. 4e, $Na_{0.65}Mn_2O_4$ specific capacity faded from 150 to 66 mAh g^{-1} after 800 cycles in pristine electrolyte, with a 43% capacity retention ratio. The capacity decay is mainly attributed to severe side reactions occurring simultaneously, as well as the uncontrolled dendritic Zn growth during cycling. In comparison, only a 26% decay of the $Na_{0.65}Mn_2O_4$ capacity occurred in the electrolyte with PFOA additives after 800 cycles under 2 A g^{-1}, and the specific capacity remained at 203 mAh g^{-1}, owing to the superior Zn reversibility. To further investigate the stability of cathode materials in the electrolyte with PFOA additives and the structural change during charge and discharge, *in-situ* Raman spectroscopy was carried out using a 532 nm laser wavelength source(Fig. 4f). Three characteristic Raman peaks were observed between 400 and 700 cm^{-1} before cycling: two in-plane Mn-O stretching vibrations along the octahedral layers between 450 and 500 cm^{-1} and out-of-plane Mn-O vibrations perpendicular to the layers around 630 cm^{-1} [36]. During the cycling process, no other obvious peaks appear and three prominent peaks remain, indicating that $Na_{0.65}Mn_2O_4$ crystal structures and Mn-O bonds were compatible in the electrolyte with PFOA additives. During the charging process, peaks around 500 and 630 cm^{-1} exhibit a red-shift, which can be attributed to a contraction of the [MnO_6] interlayer spacing due to reduced interlayer repulsion of the [MnO_6] octahedra [37], showing the de-intercalation process of Zn^{2+} in the cathode material. After that, these peaks resume to the original positions after discharging, showing the reversible interlayer spacing change. This proves that the cathode structure change in the electrolyte with PFOA additives is reversible, in line with the galvanostatic charge-discharge test results.

Molecular dynamics (MD) calculations were performed using GROMACS 2019. 3 to investigate the hydration and movement features of Zn^{2+} with and without PFOA additives in the aqueous solution at 298.15 K. Partial electric charge sets and Lennard-Jones parameters for the AMBER force field to describe the Zn^{2+} binding with water and SO_4^{2-} are shown in Table 1. The simulation results in Fig. 5 revealed that in the electrolyte with PFOA additives, PFOA molecules could occupy part of the Zn^{2+}-solvation sheath, which results in a PFOA anion-water composition of the Zn^{2+}-solvation shell. A lower coordination number of Zn^{2+} with water molecules was observed compared to the pristine zinc sulfate electrolyte from the MD results. Furthermore, according to the τ value of MD, the formation of PFOA-water-Zn^{2+} aggregates could be more beneficial for Zn^{2+} desolvation process than water-Zn^{2+} aggregates. The mean square displacement (MSD) results confirmed that the Zn^{2+} has a higher ion migration trend in the electrolyte with PFOA additives than the pristine electrolyte, which could contribute to the rate performance of AZIBs.

3. Conclusion

In this study, ultralow quantities of a fluorinated surfactant additive were introduced into aqueous electrolytes to improve the reversibility of Zn plating process and overall battery performance. The electrolyte with PFOA additives optimizes the Zn plating nucleation process by elevating

Table 1
Partial electric charge sets and Lennard Jones parameters for the AMBER force field.

	Partial electric charge sets	Mass	Lennard-Jones parameters	
			σ (Å)	ε (KJ·mol^{-1})
Zn^{2+}	2.0000	65.4	1.95998	0.523
Ss	1.540804	32.06	3.56359	0.1046
Os	-0.885201	16.00	3.00001	0.71128
Ow	-0.8476	15.9994	3.15061	0.636386
Hw	0.4238	1.0080	0.0000	0.0000
Cf	0.414326	12.01	3.39967	0.359824
Ff	-0.18277	19.00	3.11815	0.255224
Of	-0.472	16.00	2.95992	0.87864
Oh	-0.565101	16.00	3.06647	0.880314
Hf	0.464	1.008	0.0000	0.0000

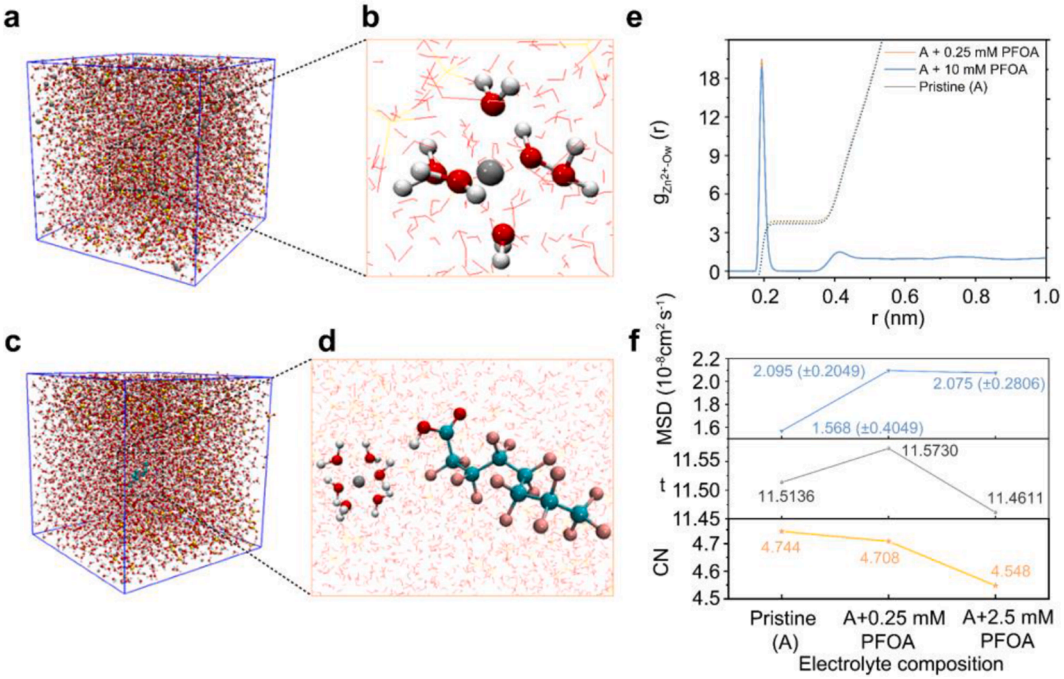

Fig. 5. (a) Molecular dynamic simulation models of pristine electrolyte. (b) H_2O molecular distribution of the Zn^{2+} first hydration layer in pristine electrolyte. (c) Molecular dynamics simulation models of electrolyte with PFOA additives. (d) H_2O molecular distribution of the Zn^{2+} first hydration layer in electrolyte with PFOA additives. Ow pair distribution function figure of Zn^{2+} (e) and water molecular (f).

nucleation overpotentials and increasing the Zn^{2+} migration by regulating the sulfate anion. Unform and dense Zn plating was observed via *in situ* optical microscopy. The absorption layer of PFOA molecules on the electrode can act as a barrier to block excessive SO_4^{2-} anion and H_2O from reaching the zinc anode, HER and OER side reactions at the interface were suppressed and the working window of the electrolyte was enlarged. MD simulations confirmed that PFOA molecules could occupy the Zn^{2+}-solvation-sheath structures. Zn^{2+} mean square displacement increased with the addition of PFOA molecules, thus proving the optimized Zn^{2+} desolvation process in the electrolyte with PFOA additives. Accordingly, the lifespan of Zn plating/stripping was extended to 2200 hand the working window increased to 2.1 V. PFOA additives can support an excellent rate performance under current densities from 0.2 to 10 mA cm^{-2} with small overpotential change. An aqueous battery consisting of $Na_{0.65}Mn_2O_4$ and Zn anode in the electrolyte with PFOA additives was assembled. The battery delivered excellent rate performance with a specific capacity of 153 mAh g^{-1} under 5 A g^{-1} and excellent cycling stability under 2 A g^{-1} with a high Coulombic efficiency. Furthermore, the interfacial wettability between electrolyte and electrode were improved, which was confirmed by decreased contract angles from 121° to 61° after adding PFOA additives. These properties indicate that PFOA can enhance the performance of both the anode and the cathode. The method of preparing electrolytes with PFOA additive is facial and cost-effective, which provides a practical solution for the large-scale application of AZIBs with high stability and reversible Zn plating/stripping. This surfactant electrolyte strategy also paves the way for promising cathode materials with high redox reaction potentials, such as Co^{2+}/Co^{3+} and Fe^{3+}/Fe^{2+}, owing to its enlarged working potential window. Such surfactant additive is expected to be a promising candidate for grid energy storage applications.

4. Experimental section

4.1. Materials

Zinc sulfate heptahydrate ($ZnSO_4{\cdot}7H_2O$, AR), Perfluorooctanoic acid ($CF_3(CF_2)_6COOH$, AR), Hydrogen Peroxide Solution (H_2O_2, 30% (w/w) in H_2O) and Polytetrafluoroethylene (PTFE) were purchased from Sigma-Aldrich (UK) Co., Ltd. Manganese sulfate (Mn_2SO_4) was purchased from Hopkin & williams (UK) Co., Ltd. YP-50F was purchased from Kuraray Chemical Company, Japan. All materials were used as received without further purification.

4.2. Electrode preparation

The sodium pre-intercalated $Na_{0.65}Mn_2O_4 \bullet 1.31H_2O$ was synthesized by a facial co-precipitation method. The cathode was fabricated by casting the mixed slurry (active material $Na_{0.65}Mn_2O_4{\cdot}1.31H_2O$, polyvinylidene difluoride (PVDF) and super P carbon in the weight ratio of 7: 1: 2, in N-methyl-2-pyrrolidone (NMP)) onto a carbon paper. These electrodes were dried in a vacuum oven for 12 h at 70 °C. The average mass loading for the dried cathodes was 1.5–2.5 mg cm^{-2}.

4.3. Materials characterization

X-ray diffraction (XRD) patterns were obtained by a Bruker-Axs X-ray D8 diffractometer (Cu-Kα radiation). with detected angular range of $2^\circ < 2\theta < 45^\circ$ with a Mo X-ray radiation source. The morphology and chemical states of the as-prepared materials and zinc plates were evaluated by scanning electron microscope (SEM; JEOL-JSM-6700F) and X-ray photoelectron spectroscopy (XPS, Thermo scientific K-alpha photoelectron spectrometer) analysis, respectively. Data processing of XPS results was achieved by Casa XPS with calibration of adventitious carbon binding energy at 284.8 eV. Raman and FT-IR data were obtained on a Raman Spectroscopy (Renishaw Raman microscope spectrometer with the laser wavelength of 514.5 nm) and Attenuated Total Reflectance Fourier transform infrared spectroscopy (ATRFTIR, BRUKER, platinum-ATR). The mass of the active materials was weighed accurately by an analytical balance (Ohaus; $\delta = 0.01$ mg).

4.4. Electrochemical evaluation

CR2032 type coin cells with different aqueous electrolytes were assembled under ambient environment. Battery performance tests were characterized by NEWARE battery testing systems for cycling stability and other electrochemical performances such as Cyclic Voltammetry (CV) and Electrochemical Impedance Spectroscopy (EIS) were measured by a VMP3 Biologic electrochemical workstation.

4.5. The details of molecular dynamics (MD) simulation

GROMACS 2019. 3 [1] was employed to investigate the hydration and movement characteristics of Zn^{2+} with or without PFOA in aqueous solution at 298.15 K. The electrostatic and Van der Waals interactions were treated using the Particle-Mesh-Ewald (PME) [2] and cut-off methods, respectively. 1.6 nm was used as the cut-off distance for electrostatic and Van der Waals interactions throughout all the energy minimization, equilibration, and production. All simulations were carried out in a periodic cubic box with lengths of 5.2 nm containing 4051 water molecules, 230 $ZnSO_4$ and 1 or 5 PFOA molecules. Each simulation was firstly equilibrated for 10 ns in the isobaric-isothermal (NPT) ensemble at 1 bar with the velocity-rescale thermostat [3] and the Berendsen coupling scheme [4]. Then, another 50 ns simulation was performed in the NPT ensemble with a time step of 1 fs. Each simulation adopted the velocity-rescale thermostat [3] and parrinello-rahman barostat [5] with relaxation time of 0.1 ps for temperature, and 1 ps for pressure. The trajectory data were collected every 5 ps for further analyses. The $ZnSO_4$, solvents and PFOA were all represented with the AMBER force field [6]. The extended simple point charge (SPC/E [7]) model were chosen for water. The visualization of molecules was displayed by the Visual Molecular Dynamics (VMD) program [8].

4.6. Estimation of the capacitive and diffusion-controlled contributions

To quantitatively evaluate the diffusion-controlled and capacitive contributions, different sweep rates of cyclic voltammetry curves were measured. Generally, the measured peak current (i) and sweep rate (ν) in CV scans obey a power-law relationship:

$$i = a\nu^b$$

thus, log(i) = log(a) + b·log(ν) where, a and b are adjustable, and the b value can be attained by fitting slope of the log(i) versus log(ν) profile. A b value of 1.0 indicates a capacitive dominated charge storage behavior while a b value of 0.5 refers to ionic diffusion-controlled behavior. Furthermore, for a quantitative analysis of diffusion-controlled and capacitive contributions in current response, assumption of an integration of semi-infinite diffusion and capacitive process were carried out by the following equation: $i = k_1\nu + k_2\nu^{1/2}$ The diffusion-controlled and capacitive contributions can be estimated by determining k_1 and k_2.

4.7. Estimation of zinc transference number

Zn^{2+} transference number was evaluated in a symmetrical Zn battery combined by EIS before and after the chronoamperometry (CA) test (shown in Supplementary Fig. S18a), and calculated by the following equation:

$$T = \frac{I_s(\Delta V - I_0R_0)}{I_0(\Delta V - I_SR_S)}$$

Where ΔV is the voltage polarization applied, I_s and R_s are the steady state current and resistance, respectively, and I_0 and R_0 are the initial current and resistance, respectively. The applied voltage polarization is 5 mV.

CRediT authorship contribution statement

Fangjia Zhao: Conceptualization, Formal analysis, Investigation, Writing – original draft. **Zhuanfang Jing:** Formal analysis, Writing – original draft. **Xiaoxia Guo:** Investigation. **Jianwei Li:** Investigation, Data curation. **Haobo Dong:** Investigation. **Yeshu Tan:** Investigation. **Longxiang Liu:** Investigation. **Yongquan Zhou:** Data curation. **Rhodri Owen:** Investigation. **Paul R. Shearing:** Funding acquisition. **Dan J.L. Brett:** Funding acquisition. **Guanjie He:** Conceptualization, Funding acquisition, Supervision, Writing – review & editing. **Ivan P. Parkin:** Funding acquisition, Supervision, Writing – review & editing.

Declaration of Competing Interest

The authors declare that they have no known competing financial interests or personal relationships that could have appeared to influence the work reported in this paper.

Data Availability

Data will be made available on request.

Acknowledgments

The authors would like to thank the Engineering and Physical Sciences Research Council (EPSRC, EP/V027433/1, EP/L015862/1, EP/R023581/1), the Royal Academy of Engineering under the Research Chairs and Senior Research Fellowships scheme (Shearing and Brett), and the Royal Society (RGS\R1\211080; IEC\NSFC\201261) for funding support. F. Zhao acknowledge A. Aliev for NMR technical support.

Supplementary materials

Supplementary material associated with this article can be found, in the online version, at doi:10.1016/j.ensm.2022.10.001.

References

[1] T. Zhang, Y. Tang, S. Guo, X. Cao, A. Pan, G. Fang, J. Zhou, S. Liang, Fundamentals and perspectives in developing zinc-ion battery electrolytes: a comprehensive review, Energy Environ. Sci. 13 (2020) 4625–4665.
[2] Y. Liu, X. Lu, F. Lai, T. Liu, P. Shearing, I. Parkin, G. He, D. Brett, Rechargeable aqueous Zn-based energy storage devices, Joule 5 (2021) 2845–2903.
[3] W. Zong, H. Guo, Y. Ouyang, L. Mo, C. Zhou, G. Chao, J. Hofkens, Y. Xu, W. Wang, Y. Miao, G. He, I. Parkin, F. Lai, T. Liu, Topochemistry-driven synthesis of transition-metal selenides with weakened Van Der Waals force to enable 3D-printed Na-Ion hybrid capacitors, Adv. Funct. Mater. 32 (2022), 202110016.
[4] K. Wu, J. Huang, J. Yi, X. Liu, Y. Liu, Y. Wang, J. Zhang, Y. Xia, Recent advances in polymer electrolytes for zinc ion batteries: mechanisms, properties, and perspectives, Adv. Energy Mater. 10 (2020), 1903977.
[5] Z. Cao, P. Zhuang, X. Zhang, M. Ye, J. Shen, M.P. Ajayan, Strategies for dendrite-free anode in aqueous rechargeable zinc ion batteries, Adv. Energy Mater. 10 (2020), 2001599.
[6] C. Liu, X. Xie, B. Lu, J. Zhou, S. Liang, Electrolyte strategies toward better zinc-ion batteries, ACS Energy Lett. 6 (2021) 1015–1033.
[7] B. Zhang, L. Qin, Y. Fang, Y. Chai, X. Xie, B. Lu, S. Liang, J. Zhou, Tuning Zn^{2+} coordination tunnel by hierarchical gel electrolyte for dendrite-free zinc anode, Sci. Bull. 67 (2022) 955–962.
[8] Z. Liu, Y. Yang, S. Liang, B. Lu, J. Zhou, pH-buffer contained electrolyte for self-adjusted cathode-free Zn–MnO_2 batteries with coexistence of dual mechanisms, Small Struct. 2 (2021), 2100119.
[9] Z. Hou, X. Zhang, X. Li, Y. Zhu, J. Liang, Y. Qian, Surfactant widens the electrochemical window of an aqueous electrolyte for better rechargeable aqueous sodium/zinc battery, J. Mater. Chem. A 5 (2017) 730–738.
[10] P. Ruan, S. Liang, B. Lu, H. Fan, J. Zhou, Design strategies for high-energy-density aqueous zinc batteries, Angew. Chem. Int. Ed. 61 (2022), e202200598.
[11] Z. Liu, L. Qin, B. Lu, X. Wu, S. Liang, J. Zhou, Issues and opportunities facing aqueous Mn^{2+}/MnO_2-based batteries, ChemSusChem 15 (2022), e202200348.
[12] X. Guo, Z. Zhang, J. Li, N. Luo, L. Chai, T. Miller, F. Lai, P. Shearing, D. Brett, D. Han, Z. Weng, G. He, I. Parkin, Alleviation of dendrite formation on zinc anodes via electrolyte additives, ACS Energy Lett. 6 (2021) 395–403.

[13] A. Bayaguud, X. Luo, Y. Fu, C. Zhu, Cationic surfactant-type electrolyte additive enables three-dimensional dendrite-free zinc anode for stable zinc-ion batteries, ACS Energy Lett. 5 (2020) 3012–3020.
[14] H. Lu, X. Zhang, M. Luo, K. Cao, Y. Lu, B. Xu, H. Pan, K. Tao, Y. Jiang, Amino acid-induced interface charge engineering enables highly reversible Zn anode, Adv. Funct. Mater. 31 (2021), 2103514.
[15] Y. Yang, C. Liu, Z. Lv, H. Yang, Y. Zhang, M. Ye, L. Chen, J. Zhao, C. Li, Synergistic manipulation of Zn^{2+} ion flux and desolvation effect enabled by anodic growth of a 3D ZnF2 matrix for long-lifespan and dendrite-Free Zn metal anodes, Adv. Mater. 33 (2021), 2007388.
[16] M. Zhou, S. Guo, J. Li, X. Luo, Z. Liu, T. Zhang, X. Cao, M. Long, B. Lu, A. Pan, G. Fang, J. Zhou, S. Liang, Surface-preferred crystal plane for a stable and reversible zinc anode, Adv. Mater. 33 (2021), 2100187.
[17] Y. Jiao, F. Li, X. Jin, Q. Lei, L. Li, L. Wang, T. Ye, E. He, J. Wang, J. Lu, R. Gao, Q. Li, C. Jiang, J. Li, G. He, M. Liao, H. Zhang, I. Parkin, H. Peng, Y. Zhang, H. Chen, Engineering polymer glue towards 90% zinc utilization for 1000 hours to make high-performance Zn-ion batteries, Adv. Funct. Mater. 31 (2021), 2107652.
[18] C. Chen, K. Matsumoto, K. Kubota, R. Hagiwara, Q. Xu, A room-temperature molten hydrate electrolyte for rechargeable zinc–air batteries, Adv. Energy Mater. 9 (2019), 1900196.
[19] S. Huang, F. Wan, S. Bi, J. Zhu, Z. Niu, J. Chen, A self-healing integrated all-in-one zinc-ion battery, Angew. Chem. Int. Ed. 58 (2019) 4313–4317.
[20] F. Wang, O. Borodin, T. Gao, X. Fan, W. Sun, F. Han, A. Faraone, J. Dura, K. Xu, C. Wang, Highly reversible zinc metal anode for aqueous batteries, Nat. Mater. 17 (2018) 543–549.
[21] Q. Zhang, J. Luan, L. Fu, S. Wu, Y. Tang, X. Ji, H. Wang, The three-dimensional dendrite-free zinc anode on a copper mesh with a zinc-oriented polyacrylamide electrolyte additive, Angew. Chem. Int. Ed. 58 (2019) 15841–15847.
[22] D. Li, L. Cao, T. Deng, S. Liu, C. Wang, Design of a solid electrolyte interphase for aqueous Zn batteries, Angew. Chem. Int. Ed. 60 (2021) 13035–13041.
[23] S. Guo, L. Qin, T. Zhang, M. Zhou, J. Zhou, G. Fang, S. Liang, Fundamentals and perspectives of electrolyte additives for aqueous zinc-ion batteries, Energy Storage Mater. 34 (2021) 545–562.
[24] Q. Zhang, Y. Hua, Effects of 1-butyl-3-methylimidazolium hydrogen sulfate-[BMIM] HSO4 on zinc electrodeposition from acidic sulfate electrolyte, J. Appl. Electrochem. 39 (2008) 261–267.
[25] W. Plieth, Electrochemistry for Materials Science, Elsevier, Amsterdam, Netherlands, 2008.
[26] D. Kashchiev, On the relation between nucleation work, nucleus size, and nucleation rate, J. Chem. Phys. 76 (1982) 5098–5102.
[27] D. Kashchiev, Forms and applications of the nucleation theorem, J. Chem. Phys. 125 (2006), 014502.
[28] Z. Zhao, J. Zhao, Z. Hu, J. Li, J. Li, Y. Zhang, C. Wang, G. Cui, Long-life and deeply rechargeable aqueous Zn anodes enabled by a multifunctional brightener-inspired interphase, Energy Environ. Sci. 12 (2019) 1938–1949.
[29] R. Yuksel, O. Buyukcakir, W. Seong, R. Ruoff, Metal-organic framework integrated anodes for aqueous zinc-ion batteries, Adv. Energy Mater. 10 (2020), 1904215.
[30] D. Hu, A. Mafi, K. Chou, Revisiting the thermodynamics of water surfaces and the effects of surfactant head group, J. Phys. Chem. B 120 (2016) 2257–2261.
[31] B. Li, X. Zhang, T. Wang, Z. He, B. Lu, S. Liang, J. Zhou, Interfacial engineering strategy for high-performance Zn metal anodes, Nanomicro Lett. 14 (2022) 1–31.
[32] P. Zou, R. Zhang, L. Yao, J. Qin, K. Kisslinger, H. Zhuang, H. Xin, Ultrahigh-rate and long-life zinc–metal anodes enabled by self-accelerated cation migration, Adv. Energy Mater. 11 (2021), 2100982.
[33] H. Dong, J. Li, S. Zhao, Y. Jiao, J. Chen, Y. Tan, D. Brett, G. He, I. Parkin, Investigation of a biomass hydrogel electrolyte naturally stabilizing cathodes for zinc-ion batteries, ACS Appl. Mater. Interfaces 13 (2021) 745–754.
[34] D. Zhang, J. Cao, X. Zhang, N. Insin, S. Wang, J. Han, Y. Zhao, J. Qin, Y. Huang, Inhibition of manganese dissolution in Mn_2O_3 cathode with controllable Ni^{2+} incorporation for high-performance zinc ion battery, Adv. Funct. Mater. 31 (2021), 2009412.
[35] L. Dai, Y. Wang, L. Sun, Y. Ding, Y. Yao, L. Yao, N.E. Drewett, W. Zhang, J. Tang, W. Zheng, Jahn–Teller distortion induced Mn^{2+}-rich cathode enables optimal flexible aqueous high-voltage Zn-Mn batteries, Adv. Sci. 8 (2021), 2004995.
[36] Z.M. Chan, D. Kitchaev, J.N. Weker, C. Schnedermann, K. Lim, G. Ceder, W. Tumas, M. Toney, D. Nocera, Electrochemical trapping of metastable Mn3+ ions for activation of MnO_2 oxygen evolution catalysts, Proc. Natl. Acad. Sci. 115 (2018) 5261–5268.
[37] T. Wu, D. Hesp, V. Dhanak, C. Collins, F. Braga, L. Hardwick, C. Hu, Charge storage mechanism of activated manganese oxide composites for pseudocapacitors, J. Mater. Chem. A 3 (2015) 12786–12795.